

Simulations of electromagnetic effects in high frequency capacitively coupled discharges using the Darwin approximation

Denis Eremin, Torben Hemke, Ralf Peter Brinkmann, and Thomas Mussenbrock

*Ruhr University Bochum, Department of Electrical Engineering and Information Sciences,
Institute of Theoretical Electrical Engineering, D-44780 Bochum, Germany*

Abstract

The Darwin approximation is investigated for its possible use in simulation of electromagnetic effects in large size, high frequency capacitively coupled discharges. The approximation is utilized within the framework of two different fluid models which are applied to typical cases showing pronounced standing wave and skin effects. With the first model it is demonstrated that Darwin approximation is valid for treatment of such effects in the range of parameters under consideration. The second approach, a reduced nonlinear Darwin approximation-based model, shows that the electromagnetic phenomena persist in a more realistic setting. The Darwin approximation offers a simple and efficient way of carrying out electromagnetic simulations as it removes the Courant condition plaguing explicit electromagnetic algorithms and can be implemented as a straightforward modification of electrostatic algorithms. The algorithm described here avoids iterative schemes needed for the divergence cleaning and represents a fast and efficient solver, which can be used in fluid and kinetic models for self-consistent description of technical plasmas exhibiting certain electromagnetic activity.

I. INTRODUCTION

Low temperature plasmas play a crucial role in materials processing [1]. Particularly capacitive radio frequency discharges are important. Such plasmas, which were first introduced in the 1960s, have undergone a continuous development keeping up with the increasing requirements of the hitech industry. One trend is the attempt to increase productivity by increasing the size of the processed wafers or substrates. In microelectronics, wafer sizes of 300 mm are now state of the art, the transition to 450 mm is envisioned [2]. The manufacturing of flat panel displays or photovoltaic solar cells requires discharges in the meter range [3–5]. The size of the processing equipment obviously must meet these requirements. A second recent trend is the use of higher, often multiple frequencies of up to few hundred MHz believed to ensure better power coupling, higher plasma density, and thus higher productivity as well [6, 7].

These developments have implications on the physical models which can be used for realistic simulations of plasma-based manufacturing processes. One such implication is of particular importance: The simultaneous increase of driving frequency, plasma density, and discharge size puts the plasmas into a regime where the commonly used “electrostatic approximation” of Maxwell’s equations no longer suffices. That means that $\nabla \times \vec{E} = 0$ (and thus $\vec{E} = -\nabla\Phi$) is not justified anymore. (In this regime the skin depth and/or wavelength of the surface waves propagating in the sheath regions may become comparable or smaller than the reactor dimension). Recent experimental studies have revealed that strong plasma and field non-uniformities appear to be connected with electromagnetic effects [8–13].

The theoretical aspects of electromagnetic effects in large-area, high frequency discharges were first systematically studied by Lieberman et al. [14]. They considered an axisymmetric slab model with uniform plasma density in the bulk and the matrix sheath (i.e., constant ion density and zero electron density), treating the plasma as a dielectric and assuming the sheath width to be constant in time. Also, a “natural boundary” condition for a CCP discharge with the dielectric sidewall that all the RF current flows through the discharge (so that the magnetic field at the sidewall is constant in the axial direction and no external source of electromagnetic excitation is involved) was employed. Under these conditions, they treated the problem analytically and gave criteria, based on the estimate of change in the power deposition profile produced by Ohmic heating due to these effects, for significance of

the standing wave and skin effects. In essence, a standing wave consists of surface waves, see, e.g., [15], excited in the cavities formed in the powered (grounded) sheath, bounded by the electrode, powered (grounded) sheath interface and the sidewall; the surface waves in the grounded and powered regions are weakly coupled with each other through the bulk. The kind of skin effect meant here manifests itself in tendency of the induced electric field in an RF-driven discharge to reduce current at the axis of the discharge and increase it close to the discharge periphery [16], similar to the skin effect in metals conducting RF current (see, e.g., [17]).

Several detailed studies were conducted by Chabert et al. [18] who used a self-consistent transmission line model to account for the interaction of RF heating and plasma density. In recent years the number of contributions to the field has multiplied, for a review see, e.g., Ref. [19].

The analytical models mentioned above, being significantly limited by the underlying assumptions, leave many important questions unanswered. Numerical simulations should be used to describe the phenomena in more realistic situations. So far a number of numerical studies based on the fluid models have been conducted for the large scale CCP discharges driven at high frequencies [20–24]. All those approaches were based on the full set of Maxwell’s equations, which contains electromagnetic radiation. The underlying equations are hyperbolic and one has to satisfy the Courant criterion on numerical stability provided an explicit algorithm, such as the popular finite-difference time-domain (FDTD) algorithm, is used for their numerical solution. The Courant criterion forces the time step to be small and the overall simulation time very long. One can resort to implicit algorithms for the numerical solution of Maxwell’s equations, however, it must be noted that the existing implicit numerical schemes are rather intricate.

In this paper we propose an alternative numerical approach for studying the large scale, high frequency driven capacitively coupled discharges, which is able to describe the electromagnetic phenomena occurring in such discharges. The approach is based on the Darwin approximation for solving the system of Maxwell’s equations [25]. The Darwin approximation reduces the original system of hyperbolic equations to a set of elliptic equations by neglecting the transversal part of the displacement current in Ampere’s law, which is justified by a scale analysis of the phenomena of interest. Since the resulting elliptic equations do not support electromagnetic radiation in vacuum, the corresponding Courant criterion

is removed and the simulation time step can be chosen as in electrostatic simulations. The required numerical scheme is a relatively simple and straightforward modification of the well-established electrostatic algorithms. Whereas numerical approaches based on the Darwin approximation have proven successful in unbounded plasmas (see, e.g., Ref. [26]), application of the Darwin approximation in plasmas having plasma-wall interfaces is more intricate. It is therefore important that the approach proposed in this article avoids the computationally expensive iterative schemes used in the previous implementations of the Darwin approximation-based algorithms for bounded plasmas (see Refs. [27–30]).

We demonstrate that the Darwin approximation is in very good agreement with the fully electromagnetic linear treatment of the problem described in [14]. However, realistic plasma density profiles are far from the model used in the latter work, hence next we study the standing wave and skin effect phenomena employing a nonlinear fluid model based on the Darwin approximation with more realistic plasma profiles treated in time domain. Unlike some works (see, e.g., Ref. [22]), which consider excitation of the electromagnetic fields in the discharge coming from external sources, we assume the “natural” excitation of the electromagnetic fields in the CCP discharge generated by the voltage/current that drives the discharge. Obviously, such kind of excitation is always present in the discharge. Also, our Darwin-fluid model accounts for finite electron inertia effects which is necessary in plasmas with low collisions driven at high frequencies.

The paper is organized as follows: In Section II we briefly describe the assumptions of the Darwin approximation and its applicability. In Section III we describe the choice of representation for the electromagnetic fields that is particularly convenient for the numerical implementation and a model geometry used in the examples studied in this paper, the boundary conditions are also given in this section. In Section IV we use a linear fluid model solving for the electromagnetic fields in frequency domain both with the Darwin approximation and the full system of Maxwell’s equations for two example cases with pronounced standing wave and skin effects, respectively, to corroborate that the Darwin approximation gives an accurate description of the phenomena in question for the parameters of interest. In Section IV we describe a nonlinear fluid model accounting for the finite electron inertia effects and also using the Darwin approximation to solve for the electromagnetic fields. We demonstrate in a model simulation the standing wave effect for a case with more realistic plasma density profiles and sheath dynamics than in cases investigated in Section IV.

Finally, we summarize the main results of our study in Section VI.

II. THE DARWIN APPROXIMATION OF THE BOLTZMANN-MAXWELL SYSTEM

In general, the electrodynamic behavior of any high frequency discharge can be described by the kinetic equation, such as Boltzmann's equation, supplemented with the system of Maxwell's equations along with appropriate boundary conditions. Reduced fluid models can be constructed from this general system by taking moments of Boltzmann's equation and postulating closure relations. The dynamics of the particle distribution function of charged species s under influence of electromagnetic forces and collisions is determined by Boltzmann's equation,

$$\frac{\partial f_s}{\partial t} + \vec{v} \cdot \nabla f_s + \frac{Z_s q_s}{m_s} \left(\vec{E} + \vec{v} \times \vec{B} \right) \cdot \nabla_v f_s = \frac{\partial f_s}{\partial t} \Big|_{\text{col}}. \quad (1)$$

In turn, the electromagnetic field is described by Maxwell's equations

$$\frac{1}{\mu_0} \nabla \times \vec{B} = \vec{j} + \epsilon_0 \frac{\partial \vec{E}}{\partial t}, \quad (2)$$

$$\epsilon_0 \nabla \times \vec{E} = -\frac{1}{c^2 \mu_0} \frac{\partial \vec{B}}{\partial t} \quad (3)$$

$$\nabla \cdot \vec{B} = 0, \quad (4)$$

$$\epsilon_0 \nabla \cdot \vec{E} = \rho, \quad (5)$$

where $\rho = \sum_s Z_s q_s \int f_s d^3v$ and $\vec{j} = \sum_s Z_s q_s \int \vec{v}_s f_s d^3v$.

Direct attempts at numerical solution of (1)-(5) usually require very long simulation time. This is connected to the fact that this system supports electromagnetic waves in vacuum, which must be resolved in explicit algorithms in order to avoid numerical instabilities. Another approach is to use an implicit algorithm for the numerical solution, where unresolved electromagnetic modes of no interest are damped numerically. However, such algorithms are cumbersome to implement and often resort to artificial numerical constructions (see, e.g., [15]).

A conceptually different alternative is to remove the stiffest time scale in electromagnetic simulation by reduction of the original system of equations using the assumption about the time and spatial scales of the expected phenomena. Namely, we use the fact that for the far most CCP discharges of interest the electrode size is small compared to the wavelength of the electromagnetic wave in vacuum corresponding to the highest frequency driving harmonics.

Following the logic of [31], one can recast (2) and (3) into a normalized form where $\epsilon = L/ct$ with L and t the typical spatial and time scale of the problem,

$$\nabla \times \vec{B} = \vec{j} + \epsilon \frac{\partial \vec{E}}{\partial t}, \quad (6)$$

$$\nabla \times \vec{E} = -\epsilon \frac{\partial \vec{B}}{\partial t}. \quad (7)$$

To the zeroth order in ϵ (7) yields $\nabla \times \vec{E} = 0$, so that to this order the electric field is purely longitudinal (irrotational); we will denote this part of the electric field \vec{E}_L . To the same order the displacement current drops out of (6). To describe the electromagnetic effects one needs to include the next order in ϵ , whereby

$$\nabla \times \vec{B} = \vec{j} + \epsilon \frac{\partial \vec{E}_L}{\partial t}, \quad (8)$$

$$\nabla \times \vec{E}_T = -\epsilon \frac{\partial \vec{B}}{\partial t}, \quad (9)$$

with \vec{E}_T the transversal (solenoidal) part of the electric field, $\nabla \cdot \vec{E}_T = 0$. (8) and (9) constitute the Darwin approximation.

One can see that this model eliminates electromagnetic waves, but keeps an important part of the physics, namely electromagnetic effects in the relatively low frequency phenomena (when the corresponding wavelength in vacuum is larger than the system size). Note that the corresponding frequencies are called (very) high frequencies in the standard terminology of the CCP discharges. It is important to note that by dropping the transversal part of the displacement current the continuity equation remains satisfied.

The relation of the Darwin model to the full system of Maxwell's equations can also be illustrated by the cold unmagnetized plasma dispersion relation in an unbounded plasma,

$$c^2 k^2 + \frac{i\omega\omega_{pe}^2}{i\omega + \nu} - \omega^2 = 0. \quad (10)$$

Fig. 1 displays the solutions $k = k(\omega)$ of this relation for a typical parameter combination ($\omega_{pe} = 2\pi \times 1$ GHz, $\nu/\omega_{pe} = 0.01$). Three distinct regimes can be discerned. Slow phenomena ($\omega \leq \nu$) are governed by the collisional skin effect $k = (1 - i)/\sqrt{2}\sqrt{\omega/\nu}\lambda_{scf}^{-1}$, with $\lambda_{scf} = c/\omega_{pe}$ the collisionless skin-depth. In the intermediate frequency range ($\nu \leq \omega \leq \omega_{pe}$), the collisionless skin effect prevails, $k = i\lambda_{scf}^{-1}$. Finally, for large frequencies ($\omega > \omega_{pe}$) this dispersion relation describes propagation of the electromagnetic waves having $k = \omega/c$.

In contrast, the dispersion relation of the Darwin model is

$$c^2 k^2 + \frac{i\omega\omega_{pe}^2}{i\omega + \nu} = 0. \quad (11)$$

The Darwin model then covers the middle ground between the electrostatic approximation and a fully electromagnetic treatment. This example, however, serves only illustrative purpose and is not general in stating that the Darwin approximation is inapplicable for $\omega > \omega_{pe}$ as the dispersion relation of waves in bounded plasmas can significantly differ from Eq. (11) (as is the case in the present study, for example). The decisive conclusion regarding applicability of the Darwin approximation for description of a phenomenon in question should be made on the basis of the smallness of the ϵ parameter defined above.

Historically, Darwin's original derivation [25] was designed to describe a set of charged particles in free space with velocities small compared to the speed of light. He started from the Lagrangian description of the N -body problem with the interaction incorporated via the retarded Lienard-Wichert potentials. A formal expansion in the smallness parameter v/c , carried up to the second order, resulted in a simplified Lagrangian with instantaneous (not retarded) potentials. In the same expansion order, relativistic corrections to the equations of motion appeared. For a recent analysis of that approach, see [32].

III. PROBLEM SETUP

For the sake of concreteness, we will consider the same problem setup for studying the standing wave and skin effect phenomena in CCP discharges as was suggested by Lieberman et al. [14], i.e., a CCP discharge having cylindrical geometry symmetric in the azimuthal direction bounded by a dielectric sidewall (see Fig. 2).

As all the numerical models described in this article will use the same field equations stemming from the Darwin approximation of Maxwell's equation, we will describe them in this section. We saw in the previous section that the electric field in the Darwin approximation is separated into two parts, a longitudinal part, which is curl-free, and a transversal part, which is divergence-free. Hence, we choose to represent the electric field in the following way,

$$\vec{E} = -\nabla\phi + \nabla \times \vec{A}_T, \quad (12)$$

where the first (second) term expresses the longitudinal (transversal) part of the electric field. The longitudinal potential ϕ is governed by Poisson's equation,

$$\nabla^2\phi = -\frac{\rho}{\epsilon_0}, \quad (13)$$

with ρ the charge density. To find an equation for the transversal vector-potential \vec{A}_T we first take the curl of Ampere's law in the Darwin approximation, which results in

$$\nabla^2\frac{\partial\vec{B}}{\partial t} = -\mu_0\nabla \times \frac{\partial\vec{j}}{\partial t}, \quad (14)$$

where we used (4). Then, one can exploit Faraday's law using the chosen representation for the transversal field,

$$\nabla \times \nabla \times \vec{A}_T = -\frac{\partial\vec{B}}{\partial t}. \quad (15)$$

Following [14], we consider only TM modes with $\vec{E} = \vec{e}_r E_r + \vec{e}_z E_z$ and $\vec{B} = \vec{e}_\theta B_\theta$, and $\vec{A}_T = \vec{e}_\theta A_{T\theta}$, so that $\nabla \cdot \vec{B} = 0$ and $\nabla \cdot \vec{A}_T = 0$ hold automatically due to the symmetry of the problem.

In all the following models we study the electromagnetic response to the “natural excitation” of a CCP discharge, prescribing a harmonically varying constant magnetic field at the sidewall, which is in agreement with the previously made assumption that all the RF

current, which drives the discharge, flows through it, and no external excitation source is involved. Correspondingly, boundary conditions for B_θ is $\partial_z B_\theta = 0$ at the electrodes ($z = -l$ and $z = l$), which is needed in order for the tangential electric field to vanish at the electrodes, and reads $B_\theta = \mu_0 I / (2\pi R)$ at the sidewall ($r = R$) (provided no RF current leaves the discharge through the dielectric sidewall). Boundary conditions for $\partial_t B_\theta$ are obtained by taking time derivative of the boundary conditions for B_θ . Further, boundary conditions for $A_{T\theta}$ are $\partial_z A_{T\theta} = 0$ at the electrodes, so that the tangential component of the transversal electric field vanishes, and $A_{T\theta} = 0$ at the sidewall. The latter boundary condition for the $A_{T\theta}$ at the sidewall can be obtained as follows. From the condition that the radial component of the transversal electric field vanishes at the dielectric sidewall one can deduce that $\partial_z A_{T\theta} = 0$ at $r = R$. Integrating this equation with respect to z at $r = R$, matching the boundary conditions for $A_{T\theta}$ at the electrodes and setting the common constant to zero, one obtains the boundary condition sought.

As the boundary conditions for the longitudinal potential will be slightly different in the two models studied in this work, we will specify the boundary conditions for each particular model separately.

IV. LINEAR MODEL PROBLEM WITH FIXED SHEATH TREATED IN FREQUENCY DOMAIN

In this section we will demonstrate that the Darwin approximation is a valid approach for investigation of the electromagnetic phenomena in CCPs by comparing the full electromagnetic solution to solution obtained with the Darwin approximation for the problem investigated by Lieberman et al. [14]. The model plasma studied there has uniform ion density and a stepwise density for the electron component, such that electrons have the same density as ions in the bulk and zero density in the sheath, the sheath boundaries are considered to be stationary. The plasma is modeled as a dielectric, change of the electric field in the sheaths due to motion of the bulk electron plasma component is modeled through the surface charge created at the interfaces between the bulk plasma and the sheath regions. This approach is valid for small oscillations of the bulk plasma (see [15]), a more general case of moving sheath boundary is considered in the next section.

Then, using the representation of the electric field given in (12) (which holds in a general case as well), one can obtain the following system of equations,

$$\nabla \times \frac{1}{\epsilon_L} \nabla \times \vec{B} = \frac{i\omega}{c^2} \nabla \times \frac{\epsilon_T}{\epsilon_L} \nabla \times \vec{A}_T \quad (16)$$

$$\nabla \times \nabla \times \vec{A}_T = -i\omega \vec{B} \quad (17)$$

provided all quantities are proportional to $e^{i\omega t}$. In (16) and (17), $\epsilon_L = 1$ in the sheath and $\epsilon_L = 1 - \omega_{pe}^2/\omega(\omega - i\nu)$ in the bulk. This system of equations describes both fully EM case (if $\epsilon_T = \epsilon_L$) and the Darwin approximation (if $\epsilon_T = 0$ in the sheath and $\epsilon_T = -\omega_{pe}^2/\omega(\omega - i\nu)$ in the bulk; this expression can be easily obtained in the usual way by using the equation of motion and Ampere's law in the Darwin approximation).

Once one obtains \vec{A}_T and \vec{B} from solution of (16) and (17), the transversal electric field can be obtained from $\vec{E}_T = \nabla \times \vec{A}_T$ and the longitudinal electric field from Ampere's law, which provides $\vec{E}_L = -ic^2/\omega\epsilon_L \nabla \times \vec{B} - \epsilon_T/\epsilon_L \nabla \times \vec{A}_T$.

Results in Figs. 3 and 4 show the power deposition profiles for two selected cases with similar parameters to the corresponding cases in [14]. In all cases $d = 2$ cm $s = 0.4$ cm, and $\nu = 10^7$ s⁻¹. The radial profiles shown in Figs. 3 and 4 are normalized values of $P_{cap} = \int_0^d |E_z|^2 dz$ (with E_z being predominantly capacitively generated electric field) and $P_{ind} = \int_0^d |E_r|^2 dz$ [14] (with E_r being predominantly induced electric field), calculated with

the full system of Maxwell's equations and the Darwin approximation. Not only do both models demonstrate same behavior qualitatively, but also quantitative difference lies within a numerical error for the parameters chosen. Consequently, from this moment on we will suppose that the Darwin approximation is a valid approach for description of the standing wave and skin effects.

V. NONLINEAR MODEL PROBLEM WITH MOVING SHEATH TREATED IN TIME DOMAIN

Although the model problem used [14] and in the previous section gives a certain insight into the standing wave and skin effects, it is still quite far from realistic CCP plasmas. The assumptions of stationary sheath boundary and stepwise electron density profile are the main drawbacks of the model. Most of the previous analytical and numerical treatments of the standing wave and skin effects in the literature also assumed stationary sheath boundary with the electrostatic sheath model (e.g., [23]), which makes the corresponding numerical algorithm faster, but strips the model of adequate description of possible nonlinear phenomena. In [24] the authors studied the problem entirely in the time domain, however, the commonly adopted drift-diffusion approximation also used in that work is clearly not applicable to the usual range of parameters in low-pressure CCP discharges, when the frequency of electron collisional momentum transfer is smaller than the driving frequency. In particular, the highly collisional regime studied in [24] renders direct comparison with results of [14] impossible, as the latter work was made under the low-collisionality ansatz.

To fully resolve the nonlinear discharge dynamics we propose another model, where the sheath boundary is allowed to move, the plasma density profiles have a more realistic shape, and the effects of finite electron mass are retained, which makes the model capable of more general treatment of the electromagnetic phenomena under question in low-pressure CCP discharges than the model considered in the previous section. The electromagnetic fields in the sheath region are calculated self-consistently with the plasma dynamics and are treated in the same way as the rest of the electromagnetic fields in the entire discharge. To keep the model simple yet comprising all the effects of interest, we adopt a fluid description for the electron plasma component, whereas ions are assumed to be immobile. To make the model realistic, we adopt the axial ion density profile from a 2D electrostatic PIC/MCC simulation (with the same geometry and plasma parameters as those of the fluid simulation studied here), taken at the half-radius radial position (since the density profiles in the electrostatic case are essentially uniform, we feel that such an approach is justified). In this way we choose to focus on the coupled dynamics of electrons and the electromagnetic fields in the entire discharge, omitting the issue of discharge sustainment. Analogously, we substitute the plasma energy balance equation with the assumption of electron isothermality. The model

geometry is the same as considered in the previous section.

The evolution of electrons is governed by the momentum equation,

$$\frac{\partial \vec{v}_e}{\partial t} + (\vec{v}_e \cdot \nabla) \vec{v}_e = -\frac{T_e}{m_e} \frac{\nabla n_e}{n_e} - \frac{e}{m_e} \left(-\nabla \phi + \nabla \times \vec{A}_T + \vec{v}_e \times \vec{B} \right) - \nu_m \vec{v}_e, \quad (18)$$

and the continuity equation,

$$\frac{\partial n_e}{\partial t} = -\nabla \cdot (n_e \vec{v}_e). \quad (19)$$

The boundary conditions for (18) is that the radial component of the electron velocity, $v_{e,r}$, vanishes at the sidewall, which comes from the assumption that all the electrons are reflected back into the discharge there, and that the axial component of the electron velocity at the driven (grounded) electrodes is $v_{e,z} = \pm 1/4 \sqrt{8k_B T_e / \pi m_e}$, respectively, which corresponds to the kinetically limited flux. The boundary conditions for (19) are, in accordance with the boundary conditions for (18), that the radial flux to the sidewall vanishes, and the axial flux to the electrodes is kinetically limited, so that $n_e v_{e,z} = \pm n_e / 4 \sqrt{8k_B T_e / \pi m_e}$ at the driven (grounded) electrodes, respectively. We take the initial ion density profile to be of the Gaussian form and the initial electron density profile to be of the same form as the ion density profile. The numerical discharge simulation gradually develops electron-depleted sheath regions (see Fig.5).

The fields are calculated self-consistently with evolution of the electron plasma component using (13) to (15)). One can distinguish two different sets of boundary conditions depending on the way the discharge is driven, either with a voltage source or a current source. Whereas boundary conditions for (15) are same for both cases (see the discussion at the end of section III), the boundary conditions for (13) and (14) are different for each case.

A. Voltage-driven discharge

In this case the potential at the driven electrode is prescribed, $\phi(z = -l) = V(t)$. This gives Dirichlet boundary condition at the driven electrode, the boundary conditions at the sidewall and the grounded electrode being same in both cases (Neumann boundary condition at the sidewall, $\partial_r \phi = 0$ and at the grounded electrode Dirichlet boundary condition $\phi = 0$. (See also the discussion in Section III).

The time derivative of the total axial current through the discharge, which enters the sidewall boundary condition for (14), must be calculated under the circumstances by inte-

grating the plasma current density time derivative, $-e\partial_t(n_e v_{e,z})$ using (18) and (19) over the surface of any discharge cross-section where the plasma current is dominant, for example, in the midplane.

B. Current-driven discharge

The potential at the driven electrode is calculate in this case from Kirchhoff's law of current continuity at the driven electrode, where the sum of the electron current and the displacement current in the sheath must match the current supplied by the source. We seek solution to ϕ in the form $\phi = (\phi_0 + \tilde{\phi}(t))\Phi_v + \Phi_\rho$, where $\nabla^2\Phi_v = 0$, where ϕ_0 is the stationary, and $\tilde{\phi}$ the harmonically changing parts of the potential at the driven electrode, respectively. The boundary conditions are: $\Phi_v = 1$ at the driven electrode, $\Phi_v = 0$ at the grounded electrode, and $\partial_r\Phi_v = 0$ at the sidewall; Φ_ρ satisfies $\nabla^2\Phi_\rho = -\rho/\epsilon_0$ with boundary conditions $\Phi_\rho = 0$ at both electrodes, and $\partial_r\Phi_\rho = 0$ at the sidewall. From the current balance at the driven electrode one has $-2\pi \int_0^R (en_e v_e + \epsilon_0 \partial_t \partial_z \phi) r dr = I(t)$. Substituting the chosen form for ϕ into this equation, one obtains an equation for the potential at the driven electrode

$$\frac{\partial \tilde{\phi}}{\partial t} = - \frac{I(t) + 2\pi \int_0^R (en_e v_{e,z} + \epsilon_0 \partial_t \partial_z \Phi_\rho) r dr}{2\pi \epsilon_0 \int_0^R (\partial_z \Phi_v) r dr} \quad (20)$$

The boundary condition for (14) at the sidewall is particularly simple in the case of current-driven discharge, as one can directly use the value of the time derivative of the total current supplied by the source.

Finally, we want to briefly discuss some details of numerical implementation of (13)), (14), (15), (18), and (19). We use a leapfrog-like scheme to integrate (18) and (19) in time, for which we use grids staggered in time for velocity and density, the density and field values being taken at integral time levels and velocity at the half- time levels. Then, the order of the whole numerical scheme is the following:

1. (18) is solved treating the nonlinear second term on the left-hand-side semi-implicitly thereby linearizing this term with respect to the density taken at the new time level. The velocity on the right hand side is time-centralized by taking the average between the new and old time levels, so that it is also semi-implicit. It is worth mentioning

that during the stage of the sheath formation an artificial viscosity term is helpful in getting rid of numerical instabilities arising at the plasma-sheath interface. Once smooth sheaths are formed, the viscosity term can be switched off.

2. The density on the right-hand side of (19) is treated semi-implicitly and is time-centralized using the same technique as in the previous procedure.
3. (13) is solved with the boundary conditions depending on the way the discharge is driven according to the techniques described above.
4. The source term in (14) should be calculated using the expression $\partial_t \vec{j}_e = -e(\vec{v}_e \partial_t n_e + n_e \partial_t \vec{v}_e)$ with $\partial_t \vec{v}_e$ and $\partial_t n_e$ calculated with help of (18) and (19). An attempt at direct evaluation of $\partial_t \vec{j}_e$ will lead to numerical instability because numerical discretization of a time derivative introduces numerical dispersion and finite field propagation time, whereas conceptually the Darwin approximation expects instantaneous field change in the whole domain (see, e.g., [33]). When calculating the source term for (14), it is also useful to write the term $\mu_0 \nabla \times e^2 n_e / m_e \nabla \times \vec{A}_T$ as $-\lambda_{\text{scf}}^2 \partial_t \vec{B} + \mu_0 e^2 n_e / m_e \nabla n_e \times \nabla \times \vec{A}_T$, where $\lambda_{\text{scf}} = c / \omega_{pe}$ is the collisionless skin depth and we used (15). The first term in this expression describes the collisionless skin effect and can be transferred to the left hand side to be treated implicitly for better numerical stability.
5. Finally, (15) is solved using the boundary conditions discussed in Section III.

One can see that because of the chosen representation for the transversal field as $\vec{E}_T = \nabla \times \vec{A}_T$ the cumbersome and computationally expensive iterative scheme needed for making sure that the calculated \vec{E}_T is divergence-free used in the previous implementations of the Darwin codes (see, e.g., [27–30]) is avoided. This is because \vec{E}_T calculated by taking the curl of \vec{A}_T guarantees that \vec{E}_T is divergence-free automatically. To account for the electromagnetic effects in 2D geometry of the problem we described, one needs to solve only two additional elliptic equations using the same field solver that is used for solving Poisson’s equation. It is a small price for removing the very expensive Courant criterion connected with propagation of the light wave, though.

In Fig. 6 we show the radial profile of relative power deposition due to the Ohmic heating by the axial electric field resulting from a current-driven discharge simulation showing a significant standing wave effect for a case with relatively low collisionality ($\nu_m = 1 \times 10^7$

s^{-1}). Parameters are similar to the parameters for the case shown on the top part of Fig. 3. The inductive power deposition is negligible and is not shown. For comparison we show results of the linear problem of the Section IV with the stepwise electron density profile and equivalent sheath width s calculated from the equation $\int_s^{l/2} dz(\bar{n}_i(z) - \bar{n}_e(z)) = \int_0^s dz \bar{n}_e(z)$ (see [34]) with the period averaged densities shown in Fig. 5. The non-uniformity of the radial power deposition profile is slightly more pronounced in the case of the nonlinear fluid model of the present Section with the more realistic electron axial density profile, but in general both models are in good agreement. Note that the radial profile of relative power deposition obtained with a purely electrostatic simulation would be uniform. As one can see, the electromagnetic component is an essential part of the standing wave effect for the parameters in question, despite the fact that surface waves propagating in sheath and generating standing waves may also exist in the electrostatic description (see, e.g., [35]).

The evidence of the model nonlinearity can be seen on the Fourier spectrum of the time-dependent voltage drop across the current-driven discharge (Fig. 7). One can clearly see that apart from the fundamental harmonic, the spectrum exhibits response at the third harmonic also. The amplitudes of other harmonics are noticeably suppressed, which might be attributed to the fact that the fluid models tend to over-relax the arising density gradients leading to damping of high harmonics.

VI. CONCLUSIONS AND OUTLOOK

In this paper we have demonstrated that the Darwin approximation is adequate for description of the standing wave and skin effects present in the high frequency CCP discharges by comparing relevant electromagnetic fields calculated using the approximation and solution of the full set of Maxwell's equations for two different typical cases exhibiting such effects in a model problem. We considered the "natural" excitation of such effects coming from the current driving the discharge needed for its very existence. The Darwin approximation reduces originally hyperbolic Maxwell's equations, by dropping the transversal current in Ampere's law, to a set of elliptic equations which do not support light waves propagating in vacuum. This has very significant consequence for the numerical algorithms based on that approach that the corresponding Courant criterion is also removed, enabling same time step size as in electrostatic algorithms. We have shown that the Darwin approximation can be straightforwardly implemented in fluid models, requiring only a slight modification of a possibly existing electrostatic code with the eventual great computational pay-off. The choice of the representation for the transversal field proposed by us helps to avoid the computationally demanding iterative schemes needed for its divergence cleaning used in other implementations. Using a reduced nonlinear fluid code self-consistently evolving plasma and electromagnetic fields in time domain, on the example of a case exhibiting standing wave effect we have shown that the electromagnetic effects persist for more realistic profiles and sheath dynamics.

The proper description of low-pressure CCP discharges ultimately requires a kinetic tool as kinetic effects are essential in such discharges. The use of the Darwin approximation is, of course, not limited to fluid models. The sheath dynamics, the heating mechanisms other than the Ohmic heating, the nonlocal transport phenomena all demand kinetic treatment. The Darwin numerical algorithm for the solution of the electromagnetic fields designed in this work can be also used in a Particle-in-Cell code. The reduced fluid model developed in this work can, in turn, serve as benchmark for such a code.

ACKNOWLEDGMENTS

The authors gratefully acknowledge fruitful discussions with Prof. R. Grauer (Ruhr University Bochum) and support by the Deutsche Forschungsgemeinschaft via the Sonderforschungsbereich TRR 87.

-
- [1] M. A. Lieberman and A. J. Lichtenberg, *Principles of Plasma Discharges and Materials Processing* (Wiley, New York, 2005), 2nd ed.F
- [2] S. Samukawa, M. Hori, S. Rauf, K. Tachibana, P. Bruggeman, G. Kroesen, J. C. Whitehead, A. B. Murphy, A. F. Gutsol, S. Starikovskaia J. Phys. D: Appl. Phys. **45** , 253001 (2012)
- [3] A. E. Park, B. U. Cho, and J. K. Lee. IEEE Trans. Plasma Sci. **31**, 628, (2003)
- [4] J. Schmitt. M. Elyaakoubi, and L. Sansonnens, Plasma Sources Sci. Technol. **11**, 206 (2002)
- [5] J. Perrin, J. Schmitt, C. Hollenstein, A. Howling, and L. Sansonnens Plasma, Phys. Control. Fusion. **42**, 353 (2000)
- [6] H. H. Goto, H. D. Löwe, and T. Ohmi, J. Vac. Sci. Technol. A **10**, 3048, (1992)
- [7] N. Nakano and T. Makabe, J. Phys. D **28**, 31, (1995)
- [8] L. Sansonnens and J. Schmitt, Appl. Phys. Lett. **82**, 182 (2003)
- [9] A. A. Howling, L. Sansonnes, J. Ballutaud, and C. Hollenstein, J. Appl. Phys **96**. 5429 (2004)
- [10] A. Perret, P. Chabert, J.-P. Booth, J. Jolly, J. Guillon, and P. Auvray, Appl. Phys. Lett. **83**, 243 (2003)
- [11] P. Chabert, J.-L. Raimbault, J.-M. Rax, and A. Perret, Phys. Plasmas **11**, 4081 (2004)
- [12] G. A. Hebner, E. V. Barnat, P. A. Miller, A. M. Paterson, and J. P. Holland, Plasma Sources Sci. Technol. **15**, 879 (2006)
- [13] P. A. Miller, E. V. Barnat, G. A. Hebner, A. M. Paterson, and J. P. Holland, Plasma Sources Sci. Technol. **15**, 889 (2006)
- [14] M. A. Lieberman, J.-P. Booth, P. Chabert, J.-M. Rax, and M. M. Turner, Plasma Sources Sci. Technol. **11**, 283 (2002)
- [15] K. J. Bowers, Thesis (PhD), UNIVERSITY OF CALIFORNIA, BERKELEY, Source DAI-B 62/07, p. 3254 (2002)
- [16] T. Mussenbrock, T. Hemke, D. Ziegler, R.P. Brinkmann, M. Klick, Plasma Sources Sci. Technol. **17**, 025018 (2008)
- [17] S. Ramo, J. R. Whinnery, and T. Van Duzer, *Fields and Waves in Communication Electronics*, 3rd ed., New York, NY: Wiley, 1994
- [18] P. Chabert, J.-L. Raimbault, J.-M. Rax, and M. A. Lieberman, Phys. Plasmas **11**, 1775 (2004)
- [19] P. Chabert, J. Phys. D: Appl. Phys. **40**, R63 (2007)

- [20] Z. Chen, S. Rauf, K. Collins, *J. Appl. Phys.* **108**, 073301 (2010)
- [21] S. Rauf, K. Bera, K. Collins, *2008 Plasma Sources Sci. Technol.* **17** 035003 (2008)
- [22] Y. Yang and M.J. Kushner, *Plasma Sources Sci. Technol.* **19**, 055011 (2010)
- [23] I. Lee, D.B. Graves, and M.A. Lieberman, *Plasma Sources Sci. Technol.* **17** 015018 (2008)
- [24] Y.-R. Zhang, X. Xu, S.-X. Zhao, A. Bogaerts, Y.-N. Wang, *Phys. Plasmas* **17** 113512 (2010)
- [25] C. G. Darwin, *Philos. Mag.*, **39**, no. 233, 537 (1920)
- [26] H. Schmitz and R. Grauer, *J. of Comp. Physics* **214**, 738 (2006)
- [27] D. W. Hewett and J. K. Boyd, *J. Comp. Phys.* **70**, 166 (1987)
- [28] D. W. Hewett, *Comp. Phys. Comm.* **84**, 243 (1994)
- [29] M. R. Gibbons and D. W. Hewett, *J. Comp. Phys.* **120**, 231 (1995)
- [30] M. R. Gibbons and D. W. Hewett, *J. Comp. Phys.* **130**, 54 (1997)
- [31] P. A. Raviart and E. Sonnendrücker, *Numer. Math* **73**, 329 (1996)
- [32] T. B. Krause, A. Apte, P. J. Morrison, *Phys. Plasmas* **14**, 102112 (2007)
- [33] C. W. Nielson and H. R. Lewis, *Methods Comput. Phys.* **16**, 367 (1976)
- [34] R. P. Brinkmann, *J. Phys. D: Appl. Phys.* **42** 194009 (2009)
- [35] D. J. Cooperberg, *Phys. Plasmas*, **5**, 853 (1998)

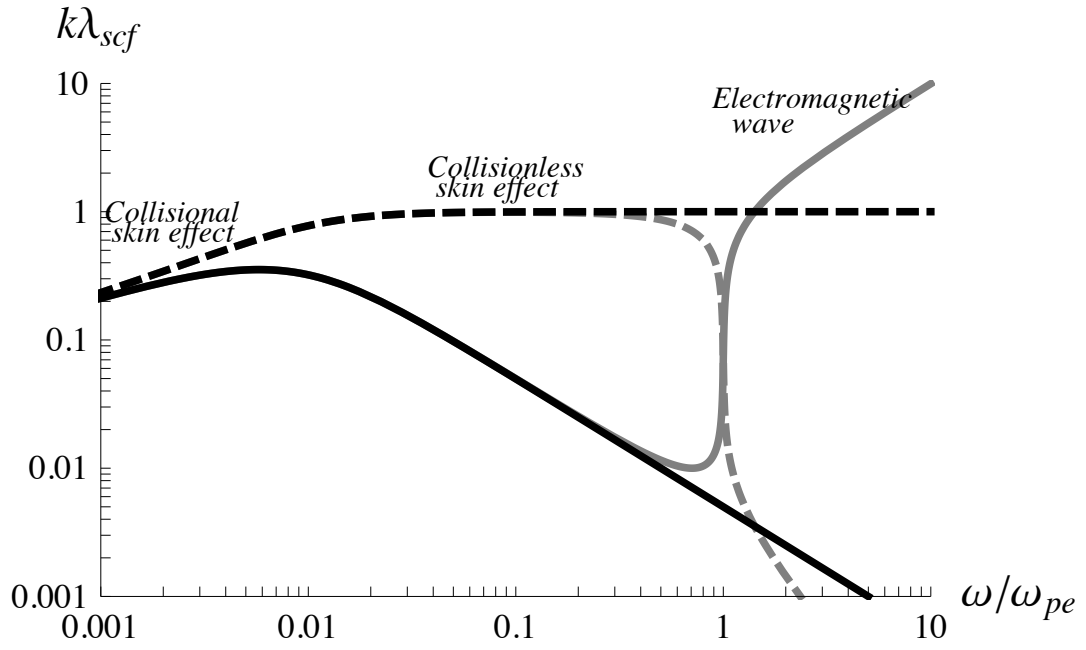


FIG. 1. The dispersion relation obtained with Darwin approximation closely follows the full electromagnetic dispersion relation as long as $\omega < \omega_{pe}$. Solid curves denote the corresponding real and dashed ones imagin

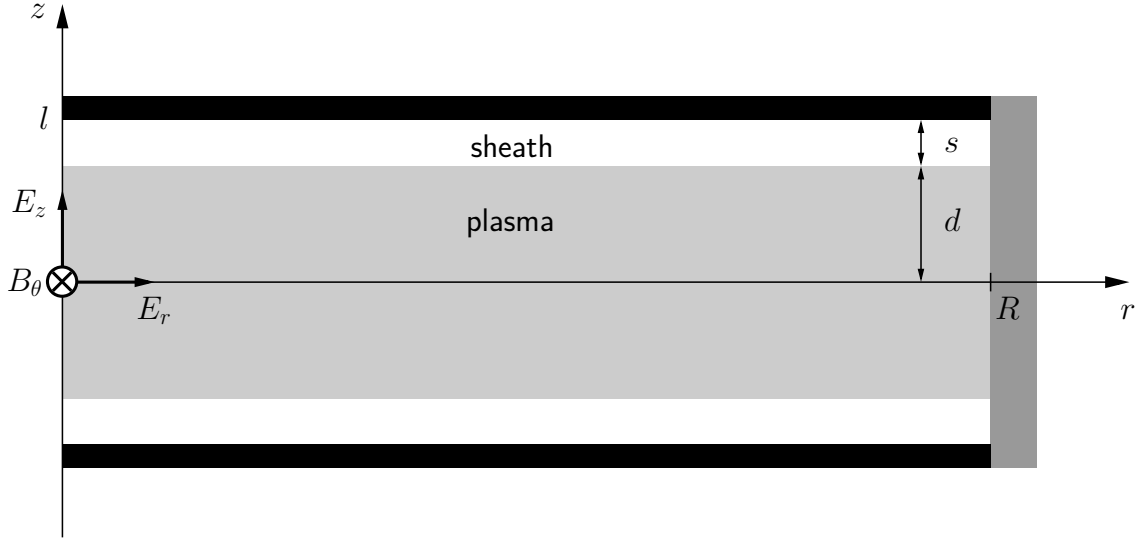


FIG. 2. Sketch of the problem geometry studied in both fluid models. The cylindrical CCP discharge under scrutiny has symmetric electrodes, a sidewall made of dielectric and a plasma. The boundary at the sheath-plasma interface is stationary in the model described in Section IV, whereas in the model of Section V it is allowed to move under the influence of electromagnetic fields. The electromagnetic fields under interest consist of the TM modes in such a plasma-filled cavity and have nonzero E_z, E_r components for the electric, and B_θ component for the magnetic fields, respectively.

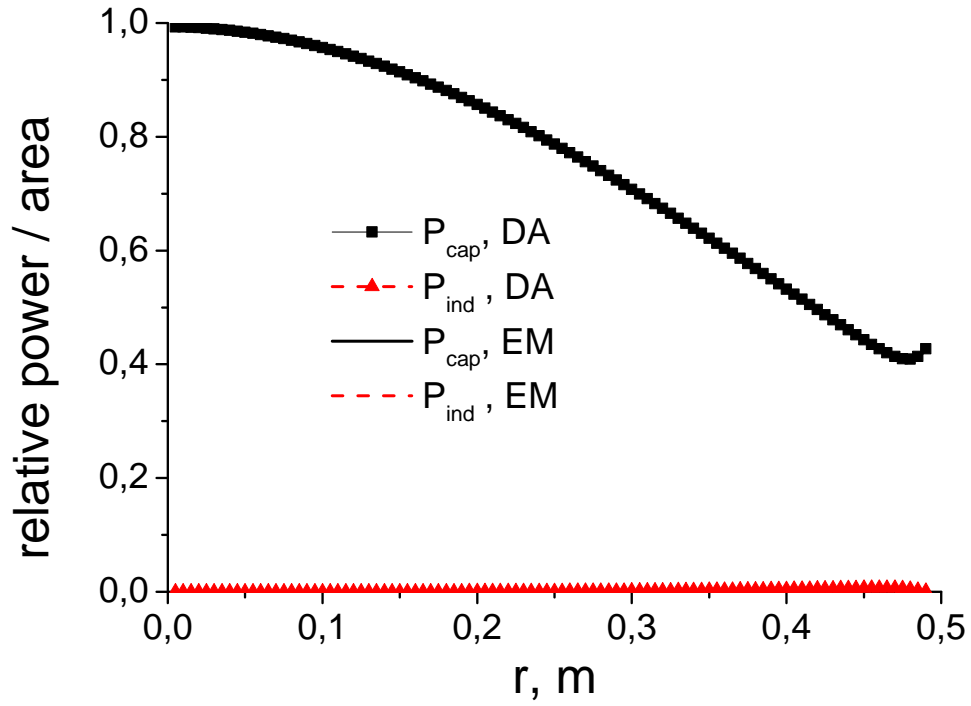


FIG. 3. Comparison of solutions obtained with Darwin approximation (DA) and full system of Maxwell's equations (EM). The first case, which exhibits a strong standing wave effect, has $f = 40,7$ MHz and $n = 10^{15} \text{ m}^{-3}$. Here $P_{cap} = \int_0^d |E_z|^2 dz$ and $P_{ind} = \int_0^d |E_r|^2 dz$, see also text.

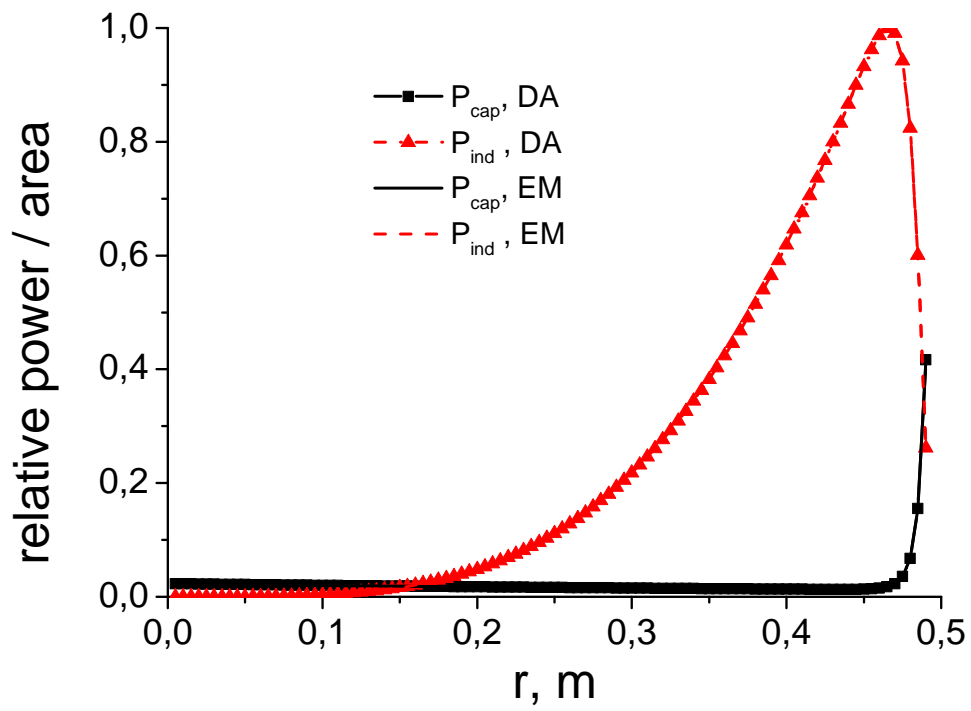


FIG. 4. The second case shows a strong skin effect and has $f = 13.56$ MHz and $n = 10^{17} \text{ m}^{-3}$.

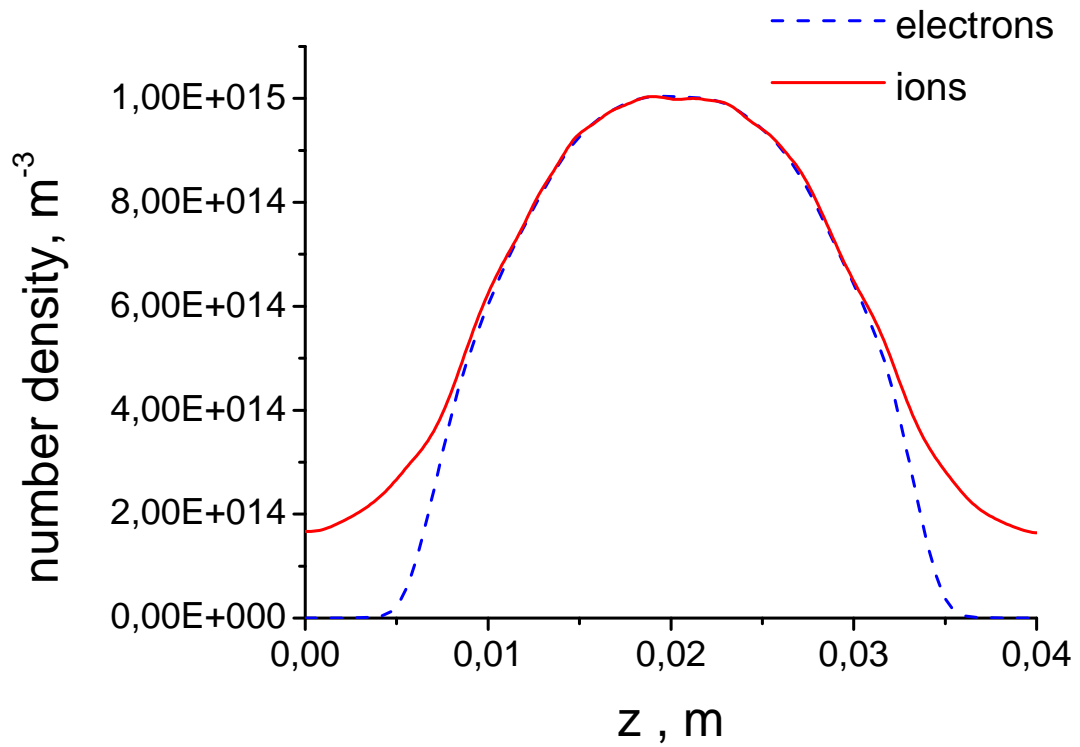


FIG. 5. In the model nonlinear simulations the ion density profile is taken from an externally conducted electrostatic PIC/MCC simulation and is held fixed, whereas mobile electrons adjust themselves to create the electron-depleted sheath regions close to the electrodes. Shown is the electron density averaged over an RF period versus the ion density profile.

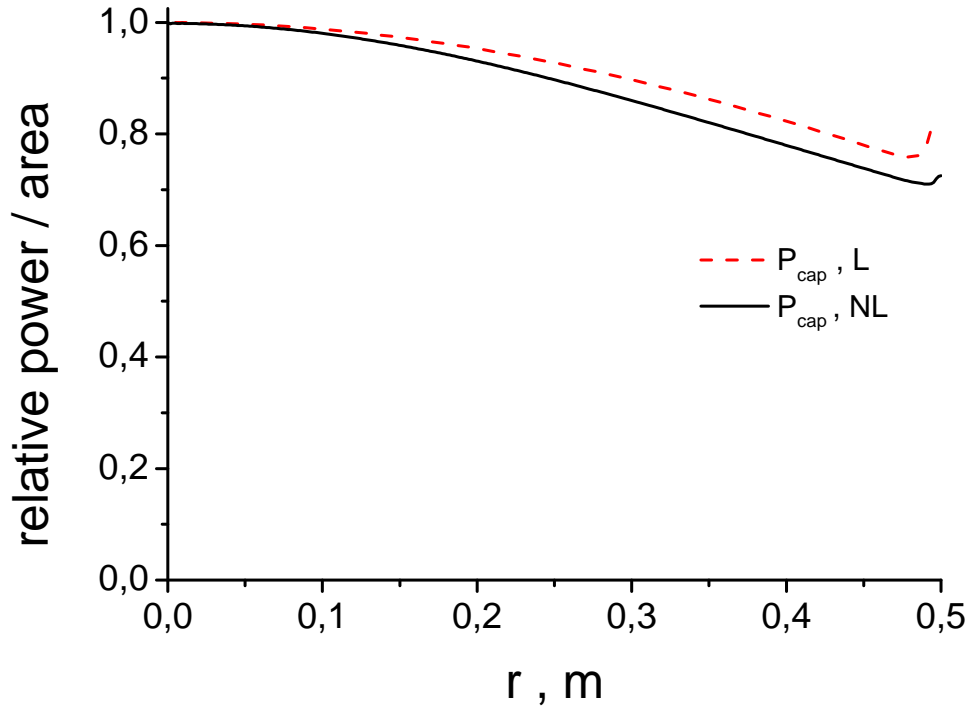


FIG. 6. Radial profile of the relative power deposition (Ohmic heating) performed by the axial electric field calculated from the nonlinear problem (black solid curve) versus results of the linear problem (red dashed curve) with the equivalent sheath width. The case shown has $f = 40.7 \text{ MHz}$ and $n_{e,max} = 1 \times 10^{15} \text{ m}^{-3}$

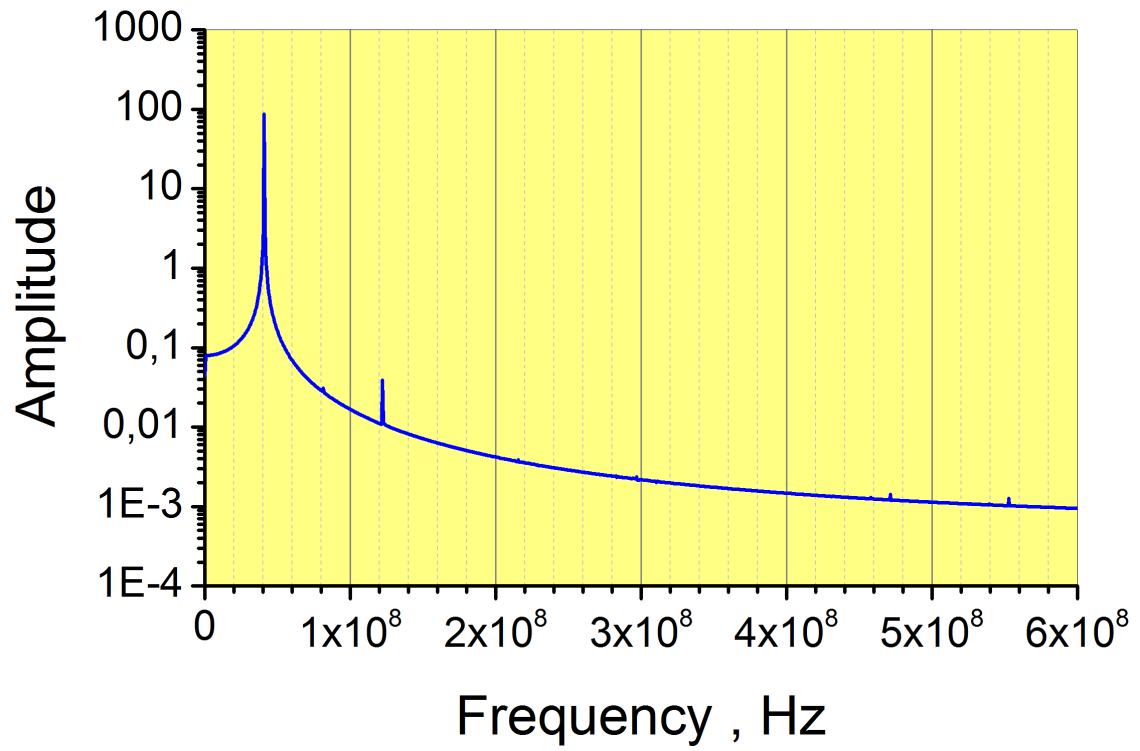


FIG. 7. Fourier frequency spectrum of the voltage drop time-dependent signal for the same current-driven discharge as shown in Fig. 6